https://doi.org/10.5194/egusphere-2026-3168
Preprint. Discussion started: 25 August 2026

A Hardware-Aware Deep Learning Framework for Wind Retrieval from Raw Doppler Spectra of Radar Wind Profilers

KyungHun Lee[1], Rackhun Son[1], ByungHyuk Kwon[1]

[1]Pukyong National University, Division of Earth Environmental System Sciences (Major of Environmental Atmospheric Sciences), Busan, South Korea

Correspondence to: Rackhun Son (rackhun@pknu.ac.kr), ByungHyuk Kwon (bhkwon@pknu.ac.kr)

Abstract. Radar wind profilers (RWPs) traditionally rely on heuristic statistical procedures for signal processing and quality control, often suffering from inherent trade-offs between data availability and retrieval reliability. To address these limitations, this study presents an end-to-end deep learning framework that retrieves wind vectors directly from raw Doppler spectra. Validated against a three-year (2022–2024) dataset of raw spectra from 437.5-MHz and 1290-MHz profiler systems and collocated radiosonde observations, the proposed framework demonstrates robust performance, particularly when trained on the full spectral continuum without filtering ambiguous samples. Notably, we found that hybridizing deep learning with conventional post-processing is highly contingent upon hardware-specific error characteristics; it effectively mitigated transient outliers in the 1290-MHz systems but provided negligible benefits for the range-smeared, vertically coherent artifacts dominating the 437.5-MHz systems. Furthermore, the framework reasonably reproduced seasonal, diurnal, and vertical atmospheric structures without the excessive smoothing typical of conventional statistical approaches. Although constrained by a slight underestimation of extreme wind speeds due to the regression-to-the-mean effect inherent in mean-squared-error optimization, the model notably enhanced operational data availability and integrity, demonstrating the feasibility of hardware-aware deep learning as a viable alternative or complement to conventional RWP processing pipelines.

https://doi.org/10.5194/egusphere-2026-3168
Preprint. Discussion started: 25 August 2026

1 Introduction

Radar wind profilers (RWPs) are remote sensing instruments that continuously observe vertical profiles of horizontal wind speed and direction by measuring the Doppler shift of signals backscattered from atmospheric turbulence and precipitation (Gage and Balsley, 1978; Strauch et al., 1984; Carter et al., 1995). Wind retrieval from received signals involves multiple signal processing stages, including coherent integration, fast Fourier transform (FFT), and incoherent integration, followed by statistical procedures such as noise estimation (Hildebrand and Sekhon, 1974; Petitdidier et al., 1997), spectral peak detection (Clothiaux et al., 1994), moment calculation (Woodman, 1985), and radial velocity consensus processing (Weber et al., 1993).

Despite these established processing procedures, RWP observations are frequently contaminated by noise and non-meteorological echoes, requiring robust quality control (QC) procedures for reliable wind retrieval (Holleman, 2005; St-James and Laroche, 2005). Various QC approaches, including adaptive filtering (Jordan et al., 1997; Boisse et al., 1999; Lehmann and Teschke, 2008) and consensus-based algorithms (Fischler and Bolles, 1981; Lambert et al., 2003), have been developed to reduce the influence of outliers and interference signals. However, conventional methods are largely based on heuristic thresholds and statistical assumptions, which often involve trade-offs between data availability and retrieval reliability. For example, extending averaging periods improves the signal-to-noise ratio (SNR) but degrades temporal resolution, whereas shorter averaging periods increase sensitivity to transient noise and outliers (Merritt, 1995; Cohn et al., 2001). In complex observational environments, multiple peaks may appear within Doppler spectra due to overlapping meteorological and non-meteorological echoes or signal broadening effects. Under such conditions, conventional peak-search algorithms often struggle to identify the meteorological spectral peak, resulting in erroneous wind retrievals (Wilczak et al., 1995; Goodrich et al., 2002). Although approaches have been proposed to address multi-peak spectra (Griesser and Richner, 1998), complex spectral structures remain a persistent challenge for heuristic retrieval methods.

https://doi.org/10.5194/egusphere-2026-3168
Preprint. Discussion started: 25 August 2026

Recent studies have increasingly applied machine learning (ML) techniques to improve signal processing and QC procedures in atmospheric remote sensing (Lolli, 2023). Neural networks have been used to classify Doppler spectra and identify non-meteorological echoes (Kretzschmar et al., 2003), while fuzzy logic and random forests have been applied to automate QC procedures and estimate atmospheric variables from RWP observations (Cornman et al., 1998; DesRosiers and Bell, 2024; Tong et al., 2024; Liu et al., 2024). However, most previous ML applications still rely on moment-based variables generated through conventional heuristic processing. As a result, these approaches inevitably inherit uncertainties and biases introduced during the initial signal processing stages. Even when raw Doppler spectra are used, previous studies have mainly focused on classification or filtering tasks rather than end-to-end wind retrieval, leaving the potential of raw spectral information for direct wind retrieval largely unexplored.

In this study, an end-to-end deep learning framework is developed to directly retrieve wind vectors from raw Doppler spectra. Using a three-year dataset of observations from 437.5 MHz and 1290 MHz RWPs along with collocated radiosonde measurements, we evaluate the retrieval characteristics of the proposed framework under different hardware configurations and signal conditions. This study further investigates how deep learning retrieval interacts with supplementary QC procedures and examines whether hardware-dependent retrieval behaviors emerge under different radar frequency characteristics. Through these analyses, this study demonstrates the potential of deep learning as a hardware-aware retrieval framework capable of complementing conventional RWP processing pipelines.

2 Data and Methodology

2.1 Observation Sites and Instruments

The Korea Meteorological Administration (KMA) operates five integrated observation sites where RWPs and radiosondes (RS) are co-located. In this study, four sites—Baengnyeongdo (BN), Deokjeokdo (DJ), Bukgangneung (BG), and Changwon (CW)—were selected for analysis, as shown in Figure 1. The Jeju site was excluded to maintain instrumental consistency, as selected sites exclusively operate standardized

https://doi.org/10.5194/egusphere-2026-3168
Preprint. Discussion started: 25 August 2026

Scintec AG systems. This exclusion mitigates potential systematic biases associated with differences in instrument architecture.

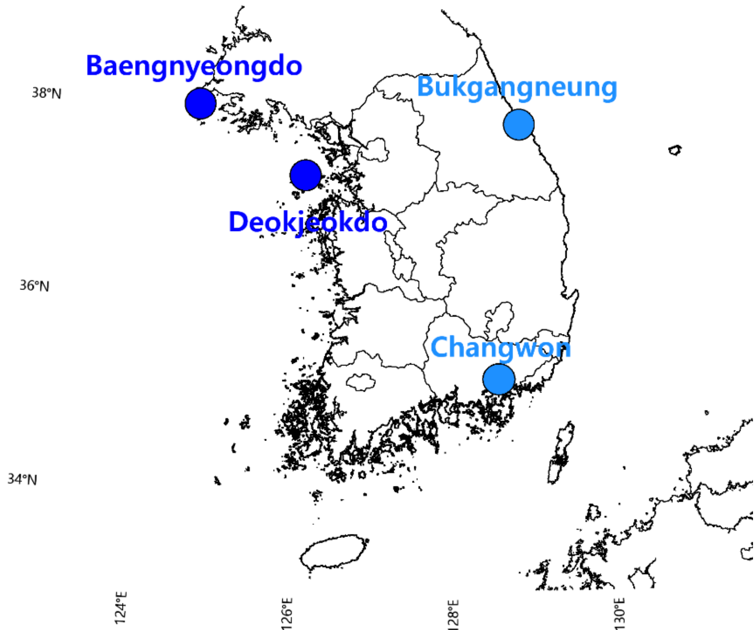

Figure 1. Geographical locations of the four RWP and RS observation sites in South Korea used in this study.

The selected sites employ two different RWP frequency bands designed for distinct observational purposes within the national observation network. The 437.5-MHz profiler (LAP-8000) systems deployed at BN and DJ are intended for deep tropospheric monitoring of synoptic-scale inflows over the West Sea. These systems are highly sensitive to Bragg scattering caused by atmospheric refractive index fluctuations and are relatively less affected by non-meteorological echoes, such as ground clutter, birds, insects, and radio frequency interference, compared to higher-frequency profilers (Weisshaupt et al., 2017). However, the long pulse width (~1165 ns) required for deep atmospheric penetration results in a relatively coarse physical range resolution of approximately 175 m. Because the observations are recorded at a gate spacing of 50 m, the systems inherently experience severe oversampling and range-smearing effects. As a result,

https://doi.org/10.5194/egusphere-2026-3168
Preprint. Discussion started: 25 August 2026

vertically redundant echoes frequently appear across adjacent range gates and multiple beam directions, producing complex multi-peak spectral structures (Figure 2) that complicate peak identification by conventional heuristic retrieval algorithms.

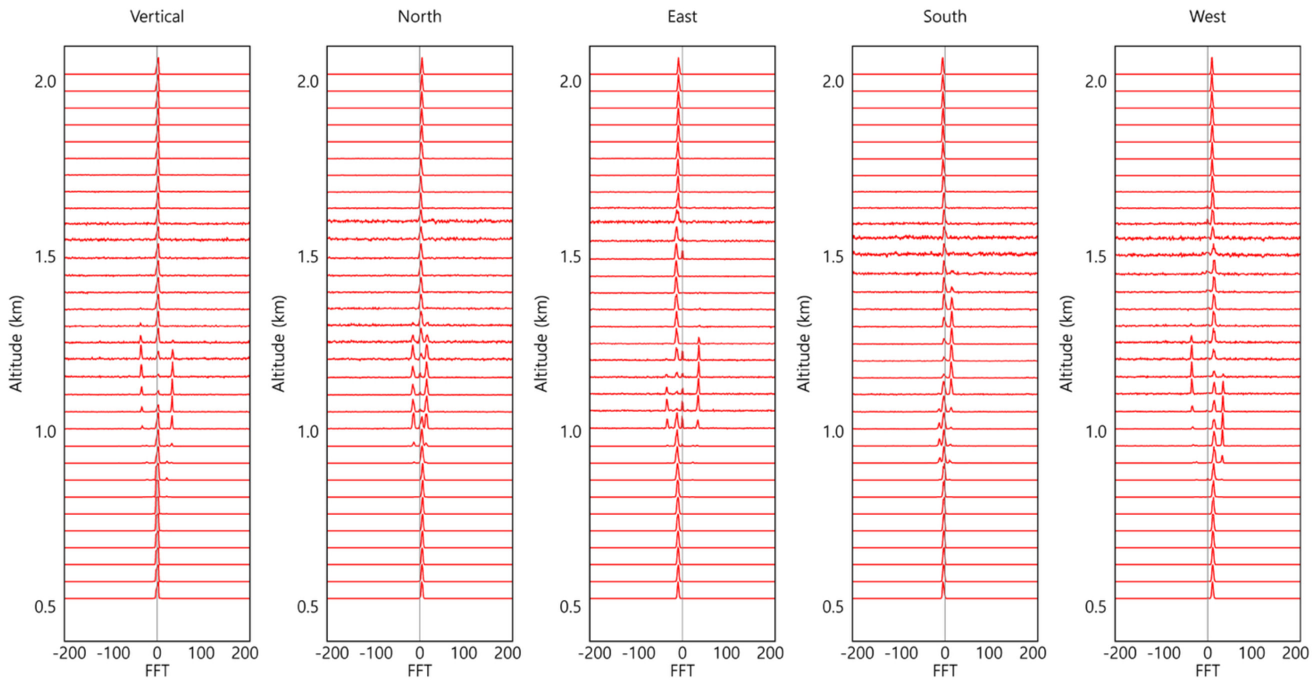

Figure 2. An example of the Doppler spectrum at the BN site (the 437.5-MHz profiler), illustrating the multi-peak phenomenon caused by the range smearing effect and oversampling of the 1165 ns pulse width.

In contrast, the 1290-MHz profiler (LAP-3000) systems deployed at BG and CW are optimized for high-resolution regional observations within the planetary boundary layer. These systems employ substantially shorter pulse widths (~400 ns), achieving a finer physical range resolution of approximately 60 m. Although this configuration enables more detailed observations of small-scale atmospheric structures, the shorter wavelength (~23 cm) makes the systems more susceptible to signal attenuation and contamination from non-meteorological echoes compared to the 437.5-MHz profiler systems (Haefele and Ruffieux, 2015). Consequently, the primary challenge for the 1290-MHz systems is not range smearing, but rather the reliable separation of meteorological signals from strong non-meteorological interference.

https://doi.org/10.5194/egusphere-2026-3168
Preprint. Discussion started: 25 August 2026

To establish reference observations for validation, RS measurements obtained using the Vaisala Autosonde system were utilized. The Autosonde system has been operational across the KMA network since 2021, with soundings conducted at either 6-hour intervals (00, 06, 12, and 18 UTC) or 12-hour intervals (00 and 12 UTC), depending on site-specific schedules. These RS observations were used to train the proposed deep learning models and to quantify the retrieval uncertainties of the RWPs. Detailed specifications and operational configurations of the RWPs at each site are summarized in Table 1.

Specification	Baengnyeongdo	Deokjeokdo	Bukgangneung	Changwon
Latitude (° N)	37.97	37.26	37.48	35.17
Longitude (° E)	124.71	126.10	128.51	128.57
Altitude (m a.s.l.)	31	9	76	40
Spectral points	423	253	393	391
Coherent integrations	6	6	7	7
Incoherent integrations	32	54	104	104
FFT points	8192	4096	2048	2048
IPP (ns)	29350	35000	31625	31475
Pulse length (ns)	1165	1165	400	400
Zenith angle (°)	15	15	15.7	15.7
Azimuth angle (°)	328	311	352	8
Frequency (MHz)	437.5	437.5	1290	1290
Beams	6	6	6	6
Temporal resolution (min)	10	10	10	10

https://doi.org/10.5194/egusphere-2026-3168
Preprint. Discussion started: 25 August 2026

Gate spacing (m)	50	50	50	50

Table 1. Specifications and operational configurations of the RWPs at the four study sites.

2.2 Data and Preprocessing

The primary input dataset consists of raw Doppler spectra obtained from the low-mode configuration of the RWPs, recorded at a temporal resolution of 10 minutes and a vertical gate spacing of 50 m. Although the standard observation cycle includes six sequential measurements across five beam directions, the present study uses a modified five-beam configuration consisting of East, North, West, South, and Vertical beams by excluding the additional vertical beam measurement to maintain consistency with the conventional wind retrieval pipeline. As reference observations, high-resolution RS data originally recorded at 1-second intervals are converted into zonal (u) and meridional (v) wind components.

To improve temporal and vertical consistency between the observations, the RWP observations are matched to the launch times of the RS soundings, while the RS profiles are vertically resampled to the 50-m range gates of the RWPs. The analysis is restricted to the altitude range between 0.5 and 2.0 km to reduce the influence of near-surface clutter and instrumental artifacts that predominantly affect lower altitudes (Meng et al., 2025), as well as representativeness errors caused by increasing RS horizontal drift at higher altitudes (Petersen and Bedka, 2007; Ingleby et al., 2016). Previous RWP–RS intercomparison studies have reported wind-component differences on the order of 1–3 m s^{-1}, although the reported magnitude varies depending on the statistical metric, instrument characteristics, comparison procedure, and observational conditions (Haefele and Ruffieux, 2015; Kottayil et al., 2016; Chen et al., 2021). These reported differences provide quantitative context for the level of disagreement that may arise when RWP and RS observations are compared.

To evaluate the proposed deep learning framework against conventional QC procedures, the outputs of the KWPP-QC algorithm developed by Lee et al. (2026) are incorporated. KWPP-QC is a multi-stage QC system composed of 13 sequential modules spanning spectral processing, moment estimation, and wind retrieval procedures. KWPP-QC was adopted as the conventional RWP processing pipeline for comparison because previous evaluation using collocated RS observations showed overall improved retrieval performance relative to operational KMA RWP products. The resulting QC outputs are used both to classify spectral environments according to signal integrity (Sect. 2.3.3.3) and to evaluate the wind retrieval performance of the proposed framework.

2.3 Deep-learning-based Quality Control Framework

2.3.1 Input Features and Target Variables

The proposed deep learning framework uses raw Doppler spectra as the primary input features. By utilizing the full spectral distribution rather than summarized statistical moments, the model is designed to learn spectral patterns associated with meteorological and non-meteorological echoes at each vertical gate. Secondary moment variables, including SNR, radial velocity, and spectral width, are intentionally excluded from the input features. This design is adopted because the information contained in these variables is inherently represented within the raw spectral density and because the study aims to establish a direct end-to-end retrieval framework that reduces dependence on intermediate heuristic processing.

The target variables consist of *u* and *v* wind components within the altitude range of 0.5–2.0 km. Model training is performed by minimizing the mean squared error (MSE) between the retrieved wind components and the spatiotemporally collocated RS observations. Through this supervised learning framework, the model learns the relationship between Doppler spectral structures and corresponding wind components while simultaneously performing signal discrimination and wind retrieval.

2.3.2 Data Splitting Strategy

To evaluate model generalization while minimizing temporal data leakage, the three-year collocated dataset is divided into training and independent test datasets using a systematic temporal splitting strategy. Unlike randomized splitting, which can artificially inflate model performance in atmospheric time-series

https://doi.org/10.5194/egusphere-2026-3168
Preprint. Discussion started: 25 August 2026

data, the adopted approach accounts for the temporal autocorrelation of wind fields associated with diurnal cycles and synoptic-scale weather variability (Thomann and Barfield, 1988; Brett and Tuller, 1991). To minimize temporal dependencies between the training and test datasets, a one-day buffer period is imposed at each transition point.

Specifically, the training dataset comprises data from the 1st to the 10th and from 22nd to the end of each month, while the test dataset consists of data from the 12th to the 20th. The 11th and 21st of each month are excluded as buffer days between the two datasets. After removing missing and corrupted samples, the final training and test datasets accounted for approximately 67% and 33% of the total data, respectively. Detailed data allocation information for each observation site is summarized in Table 2.

Site name	Data period	Total (months)	Train (%)	Test (%)
Baengnyeongdo	2022: Jan, Mar–Aug, Dec 2023: Jan–Nov 2024: Jun–Nov	25	67.6	32.4
Deokjeokdo	2022: Dec 2023: Jan–Nov 2024: Jun–Dec	19	66.8	33.2
Bukgangneung	2022: Jan–Dec 2023: Jan–Nov 2024: Jun–Dec	30	67.1	32.9
Changwon	2022: Jan–Apr, Jun, Aug–Dec 2023: Jan–Nov 2024: Jun–Dec	28	66.8	33.2

Table 2. Data splitting strategy for the training and test datasets at each observation site, including the specific data periods and allocation ratios.

https://doi.org/10.5194/egusphere-2026-3168
Preprint. Discussion started: 25 August 2026

2.3.3 Model Architecture and Configurations

The proposed deep learning architecture, illustrated in Figure 3, adopts a multi-scale feature extraction strategy tailored for one-dimensional Doppler spectral inputs. Each input sample consists of raw spectral intensities across FFT frequency bins. The framework comprises two primary components: a multi-branch convolutional feature extractor and a subsequent feature fusion network.

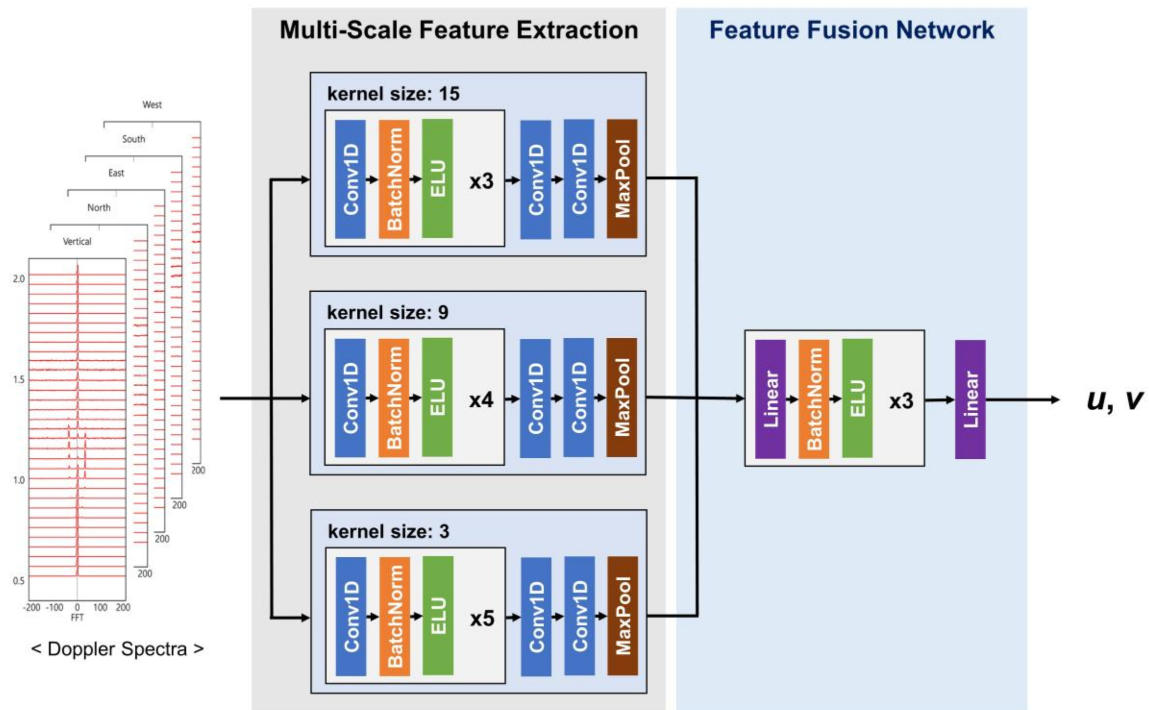

Figure 3. Schematic illustration of the proposed deep learning architecture for wind retrieval from raw Doppler spectra.

2.3.3.1 Multi-Scale Feature Extraction

To capture spectral patterns across multiple receptive fields, the input spectra are processed in parallel through three independent convolutional branches with kernel sizes of 15, 9, and 3, respectively. These

https://doi.org/10.5194/egusphere-2026-3168
Preprint. Discussion started: 25 August 2026

branches are designed to extract features ranging from broad spectral structures to fine-scale local variations.

Each branch consists of convolutional blocks incorporating batch normalization (Ioffe and Szegedy, 2015), and exponential linear unit (ELU) activation function (Clevert et al., 2015). Max pooling layer with a kernel size of 3 and a stride of 2 is applied for spatial dimensionality reduction and translation invariance. The final layer of each branch compresses the extracted features into a fixed-length latent representation (d_{hidden} = 128).

2.3.3.2 Feature Fusion Network

The feature maps generated by the three convolutional branches are flattened and concatenated into a unified feature vector, which is subsequently processed by the feature fusion network. This network consists of three fully connected layers, each followed by batch normalization and ELU activation function. The final linear layer projects the latent representation onto a two-dimensional output space (d_{out} = 2), corresponding to the predicted *u* and *v* wind components.

2.3.3.3 Data Flagging and Model Experimental Design

To construct the training datasets described in Sect. 2.2, a tiered quality-flagging system derived from the moment-level QC modules of the KWPP-QC algorithm (Lee et al., 2026) is utilized. The classification is based on the sequential outputs of Module 8 (low-SNR filtering), Module 9 (radial velocity vertical discontinuity check), and Module 10 (radial velocity consensus check). Each radial velocity sample is assigned one of three categorical flags according to its processing history.

- Uncertain: Regions initially filtered by Modules 8 or 9 but subsequently restored through the consensus procedure in Module 10. These regions represent spectrally ambiguous environments in which meteorological and non-meteorological echoes coexist, making reliable peak identification difficult for conventional heuristic retrieval methods.

https://doi.org/10.5194/egusphere-2026-3168
Preprint. Discussion started: 25 August 2026

- Certain: Regions that maintained valid radial velocity estimates throughout the entire QC sequence up to Module 10 without being classified as missing values. These regions generally correspond to dominant meteorological echoes with relatively stable spectral characteristics.
- Rejected: Regions ultimately classified as non-meteorological echoes or statistically invalid signals during the KWPP-QC procedure and assigned as missing values. These regions are primarily associated with noise, ground clutter, or other non-meteorological contamination.

Based on these flagged datasets, three deep learning models are developed to evaluate the influence of signal quality on retrieval behavior.

- DL-v1 (Uncertain-only): Trained exclusively using spectral samples containing at least one beam classified as "Uncertain." This model was designed to evaluate the capability of deep learning retrieval under ambiguous spectral environments.
- DL-v2 (Certain-only): Trained exclusively using samples classified as "Certain" across all five beams. This model is intended to evaluate retrieval performance under relatively stable meteorological conditions using signals classified as valid by KWPP-QC10.
- DL-v3 (comprehensive model): Trained using the combined set of "Uncertain" and "Certain" samples while excluding "Rejected" data. This model represents the primary end-to-end retrieval framework evaluated in this study.

This multi-model experimental design enables an investigation of how retrieval performance varies according to spectral signal characteristics and QC conditions. While DL-v1 and DL-v2 are used to examine retrieval behavior under contrasting signal environments, DL-v3 is adopted as the primary model for comparison with the KWPP-QC baseline.

To further evaluate operational applicability, the spatiotemporal continuity checks corresponding to Modules 11–13 of KWPP-QC are additionally applied as a post-processing procedure to the DL-v3

https://doi.org/10.5194/egusphere-2026-3168
Preprint. Discussion started: 25 August 2026

retrievals. This integrated framework is hereafter referred to as DL-QCv3. Comparisons between DL-QCv3 and the final KWPP-QC outputs are subsequently performed to assess the complementary roles of deep learning retrieval and conventional QC procedures.

3 Results and Discussion

3.1 Performance Evaluation of the Deep Learning Models

3.1.1 Comparative Performance across Signal Categories

To evaluate the retrieval performance of the proposed deep learning models, the conventional heuristic algorithm KWPP-QC10 is first adopted as the baseline reference (Table 3). The baseline results exhibit clear site- and frequency-dependent error characteristics. At the 1290-MHz profiler sites (BG and CW), where non-meteorological contamination is more pronounced, KWPP-QC10 shows relatively large retrieval errors, particularly in the *v* wind component, with RMSE values reaching 3.60 m s−1 and correlation coefficients decreasing to 0.77. At the 437.5-MHz profiler sites (BN and DJ), retrieval performance is comparatively more stable; however, RMSE values of approximately 2.5–3.0 m s−1 still remain due to spectral ambiguity associated with lower range resolution and range-smearing effects. In addition, systematic biases persist across most sites, with MBE values ranging from −0.47 to 0.50 m s−1.

The retrieval characteristics of the deep learning models vary depending on the spectral environments included in the training datasets. DL-v1, trained using only samples containing at least one “Uncertain” beam, showed limited improvements at the 437.5-MHz profiler sites, where “Uncertain” samples accounted for only ~1 % of the total dataset. In contrast, more noticeable improvements are observed at the 1290-MHz profiler sites, where the proportion of “Uncertain” samples increased to approximately 12 %, indicating that learning from spectrally ambiguous samples contributed more effectively in clutter-prone environments. At BG, DL-v1 substantially reduces retrieval errors, whereas at CW, improvements are primarily reflected in reduced MBE rather than RMSE, suggesting a statistical rather than physical improvement in retrieval accuracy.

https://doi.org/10.5194/egusphere-2026-3168
Preprint. Discussion started: 25 August 2026

DL-v2, trained exclusively using "Certain" samples across all five beams, exhibits a different retrieval tendency. At the 437.5-MHz profiler sites, DL-v2 consistently improves correlation coefficients while reducing RMSE values to 1.73–2.01 m s−1. These improvements suggest that DL-v2 can more effectively handle multi-peak ambiguities associated with range-smearing effects than the conventional heuristic framework, even within spectral regions pre-classified as "Certain". However, performance improvements at the 1290-MHz profiler sites remain relatively limited. Furthermore, the MBE patterns of DL-v2 closely resembled those of KWPP-QC10 across all sites, suggesting that DL-v2 retains similar systematic retrieval characteristics with the conventional framework since it is trained solely on pre-filtered high-confidence samples.

Among the tested configurations, DL-v3 demonstrates the most consistent retrieval performance across all observational environments. By utilizing both "Certain" and "Uncertain" samples, DL-v3 maintains the enhanced correlation and reduced RMSE achieved by DL-v2 at the 437.5-MHz profiler sites while substantially reducing systematic bias. At the 1290-MHz profiler sites, DL-v3 also outperforms DL-v1 and DL-v2, particularly at BG. These results indicate that incorporating the full range of valid spectral conditions improves retrieval robustness across heterogeneous observational environments.

Site name	Metric	KWPP-QC10		DL-v1		DL-v2		DL-v3	
		u	*v*	*u*	*v*	*u*	*v*	*u*	*v*
Baengnyeongdo	R	0.88	0.91	0.88	0.91	0.95	0.96	0.95	0.96
	RMSE ($m\ s^{-1}$)	2.64	2.97	2.63	2.93	1.79	1.91	1.76	1.86
	MBE ($m\ s^{-1}$)	-0.41	-0.23	0.03	-0.01	-0.38	-0.22	0.01	-0.03
Deokjeokdo	R	0.91	0.91	0.90	0.91	0.95	0.94	0.95	0.94
	RMSE ($m\ s^{-1}$)	2.53	2.66	2.53	2.66	1.73	2.01	1.74	2.01

https://doi.org/10.5194/egusphere-2026-3168
Preprint. Discussion started: 25 August 2026

	MBE (m s^{-1})	-0.40	0.50	0.02	0.01	-0.40	0.49	0.04	0.02
Bukgangneung	R	0.88	0.77	0.89	0.81	0.89	0.76	0.90	0.83
	RMSE (m s^{-1})	3.07	3.56	2.81	2.87	2.91	3.36	2.61	2.62
	MBE (m s^{-1})	-0.01	0.1	0.04	0.05	0.01	0.15	0.02	0.01
Changwon	R	0.89	0.85	0.88	0.85	0.89	0.84	0.89	0.85
	RMSE (m s^{-1})	3.00	3.60	3.06	3.46	2.95	3.60	2.99	3.44
	MBE (m s^{-1})	-0.47	0.06	0.01	0.01	-0.41	0.06	-0.06	0.05

Table 3. Statistical performance metrics (R, RMSE, and MBE) of KWPP-QC10 and the three deep learning models (DL-v1, DL-v2, and DL-v3) for the *u* and *v* wind components across the four observation sites.

To further examine whether the proposed models preserve atmospheric variability without excessive statistical smoothing, normalized Taylor diagrams are analyzed, consistently showing distinct radar-frequency-dependent-characteristics (Figure 4). At the 437.5-MHz profiler sites, DL-v2 and DL-v3 cluster closest to the RS reference point, exhibiting higher correlations and reduced centered RMSE values compared to KWPP-QC10 and DL-v1. In contrast, at the 1290-MHz profiler sites, the performance hierarchy generally follows the order of DL-v3 > DL-v1 > DL-v2 > KWPP-QC10, indicating that retrieval improvements in clutter-prone environments are strongly associated with learning from spectrally ambiguous samples. Overall, by maintaining normalized standard deviations close to the observational reference while simultaneously reducing centered RMSE, DL-v3 demonstrates improved agreement with observed atmospheric variability across different spectral environments.

https://doi.org/10.5194/egusphere-2026-3168
Preprint. Discussion started: 25 August 2026

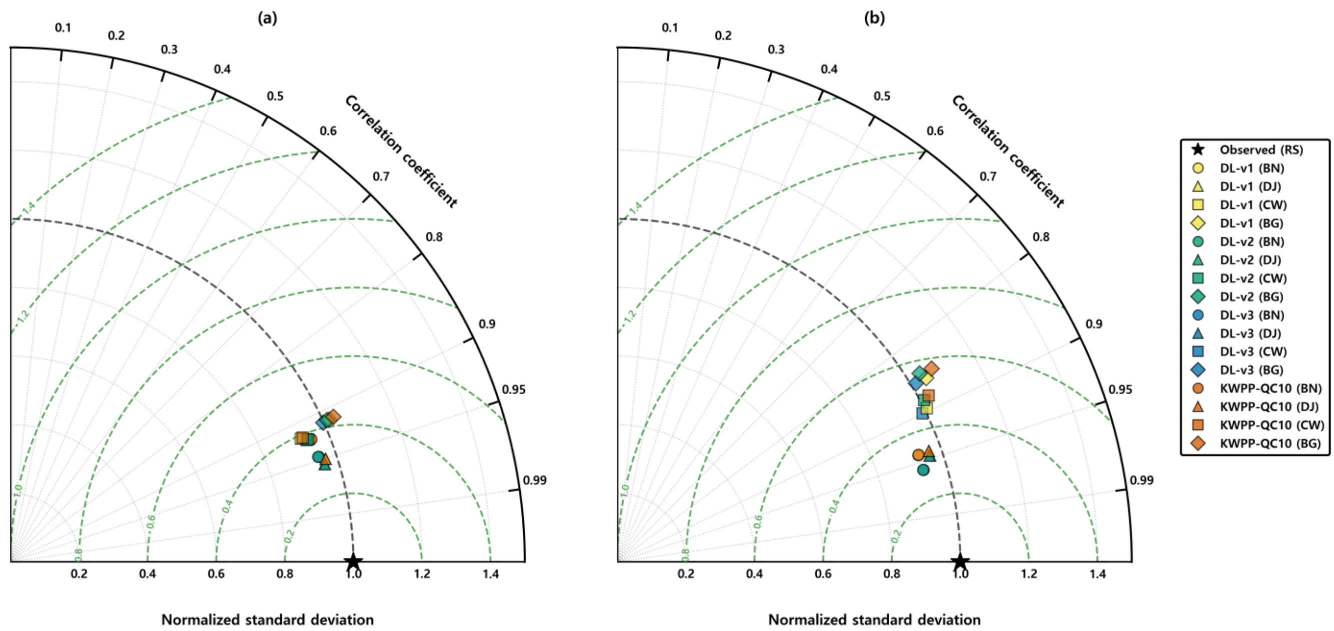

Figure 4. Normalized Taylor diagrams comparing the performance of the three deep learning models (DL-v1, DL-v2, DL-v3) and KWPP-QC10 against RS observations for the (a) *u* and (b) *v* wind components.

3.1.2 Retrieval Performance within Signal-Masked Subsets

To further evaluate the retrieval characteristics of the comprehensive model, DL-v3 is compared with the subset-trained models (DL-v1 and DL-v2) within their corresponding signal subsets. Within the "Uncertain" signal regimes, DL-v1 consistently exhibits larger retrieval errors than DL-v3 across all observation sites, with the differences being particularly pronounced at BN and DJ (Figure 5a). Although DL-v1 was trained exclusively on spectrally ambiguous samples, DL-v3 maintained more stable retrieval performance by learning from the broader spectral continuum that included both high- and low-quality signals. These results suggest that isolated low-quality spectra alone provide insufficient context for stable wind retrieval, and that incorporating the full spectral context improves retrieval robustness under ambiguous conditions.

https://doi.org/10.5194/egusphere-2026-3168
Preprint. Discussion started: 25 August 2026

A separate comparison is conducted within the “Certain” signal regimes to evaluate whether the inclusion of “Uncertain” samples during training degraded retrieval performance under relatively stable spectral conditions. As shown in Figure 5b, DL-v3 maintains retrieval performance comparable to that of DL-v2 across all sites, without statistically significant increases in retrieval error. This indicates that the comprehensive model remains stable even when trained using spectrally heterogeneous datasets containing both reliable and ambiguous samples.

Overall, these findings demonstrate that retrieval performance benefits from learning across the full range of valid spectral conditions rather than from training on spectrally isolated subsets. The integrated learning strategy adopted in DL-v3 therefore provides the most consistent retrieval behavior across heterogeneous observational environments. Based on these results, DL-v3 is selected as the primary model for subsequent analyses.

https://doi.org/10.5194/egusphere-2026-3168
Preprint. Discussion started: 25 August 2026

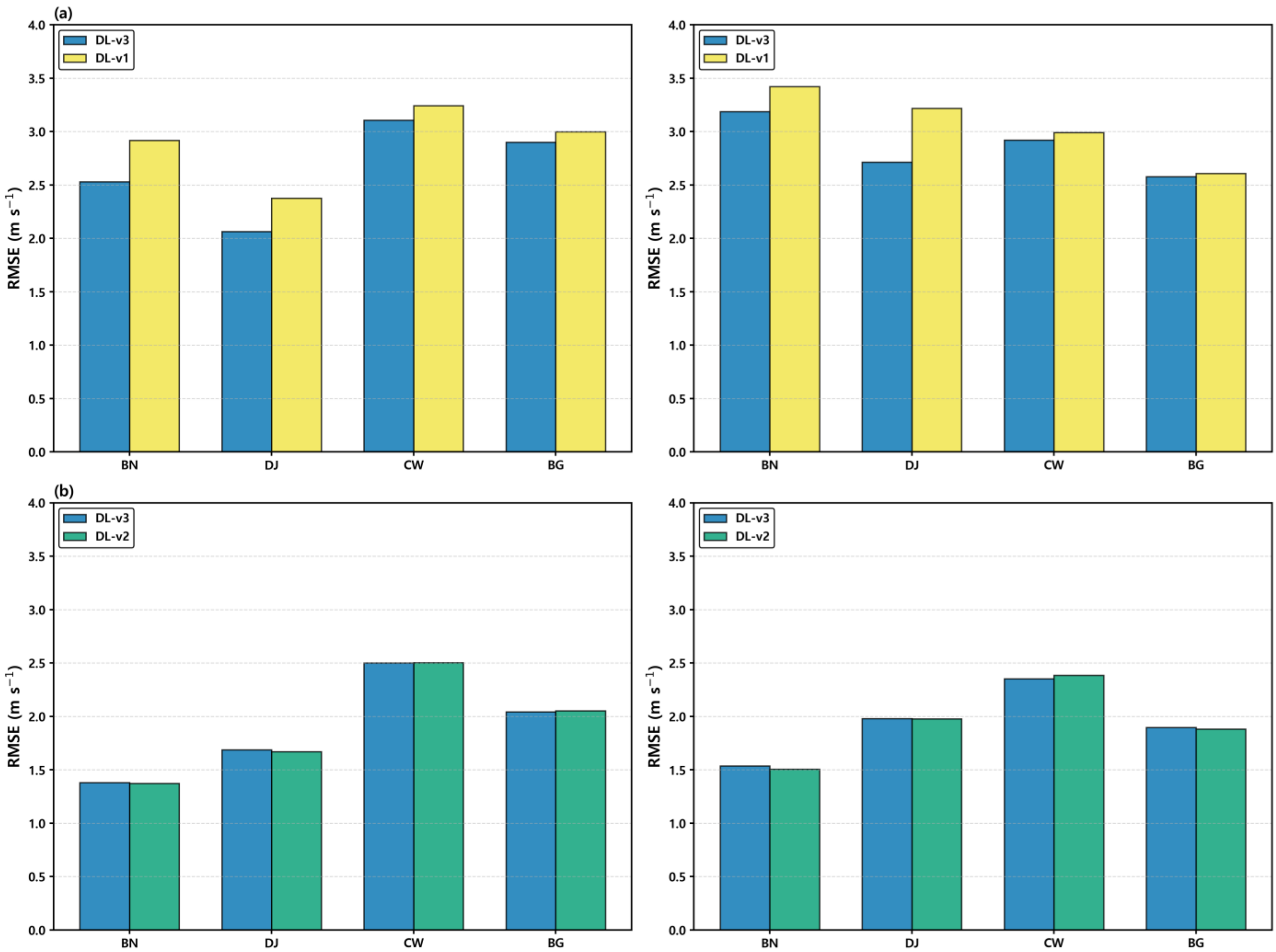

Figure 5. Comparison of RMSE for the *u* and *v* wind components among the three deep learning models in specific masked regions across four sites. (a) Performance of DL-v3 versus DL-v1 in the 'Uncertain' region. (b) Performance of DL-v3 versus DL-v2 in the 'Certain' region.

3.2 Synergy between Deep Learning and Conventional Post-processing

To investigate the potential synergy between deep learning retrieval and conventional heuristic QC procedures, the spatiotemporal post-processing modules of KWPP-QC—including wind continuity inspection, linear interpolation, and consensus-based filtering (Modules 11–13)—are additionally applied

https://doi.org/10.5194/egusphere-2026-3168
Preprint. Discussion started: 25 August 2026

to the DL-v3 retrievals. This integrated framework, DL-QCv3, is compared with KWPP-QC10, KWPP-QC13, and the standalone DL-v3 model across the four observation sites (Figure 6).

At the 1290-MHz profiler sites (BG and CW), substantial retrieval improvements are observed as the processing advanced from KWPP-QC10 to KWPP-QC13. As described in Sect. 2.1, the 1290-MHz profiler systems are highly susceptible to non-meteorological echoes, which frequently appear as spatiotemporally discontinuous outliers. The improved performance of KWPP-QC13 therefore indicates that the continuity-based post-processing procedures are effective at identifying and filtering these transient contamination signals. Although the standalone DL-v3 model still exhibited larger retrieval errors than KWPP-QC13 in certain 1290-MHz cases, the integrated DL-QCv3 framework achieves the best overall performance, particularly at CW. These results suggest that combining deep learning retrieval with spatiotemporal continuity-based QC procedures provides complementary benefits in clutter-prone observational environments.

In contrast, the 437.5-MHz profiler sites (BN and DJ) exhibit a markedly different behavior. Although KWPP-QC13 improves upon KWPP-QC10, the standalone DL-v3 model already produces substantially lower retrieval errors than the conventional QC framework. Furthermore, the additional application of Modules 11–13 produced only marginal differences between DL-v3 and DL-QCv3, with slight error increases noted for the *v* wind component at BN. This limited synergy suggests that the dominant error characteristics of the 437.5-MHz profiler systems fundamentally differ from those of the 1290-MHz profiler systems. As discussed in Sect. 2.1, the primary challenge in the 437.5-MHz environments arises from vertically coherent multi-peak structures generated by range-smearing effects rather than from isolated discontinuous outliers. Because continuity-based post-processing procedures are originally designed to remove transient outliers, their effectiveness becomes limited once the major spectral ambiguities have already been resolved by the deep learning retrieval framework.

These results demonstrate that the effectiveness of integrating conventional QC with deep learning retrieval is strongly conditioned by the dominant error characteristics of the radar system, highlighting

https://doi.org/10.5194/egusphere-2026-3168
Preprint. Discussion started: 25 August 2026

the necessity of hardware-aware pipeline design. At the 437.5-MHz profiler sites, where DL-v3 and DL-QCv3 consistently outperform the conventional QC framework, the findings further suggest that the deep learning framework successfully retrieves meteorological signals that are not adequately resolved by the heuristic processing pipeline. The following section therefore examines how DL-QCv3 reconstructs meteorological wind structures in retrieval regions where conventional heuristic QC frequently produces missing values or erroneous retrievals under severe range-smearing conditions.

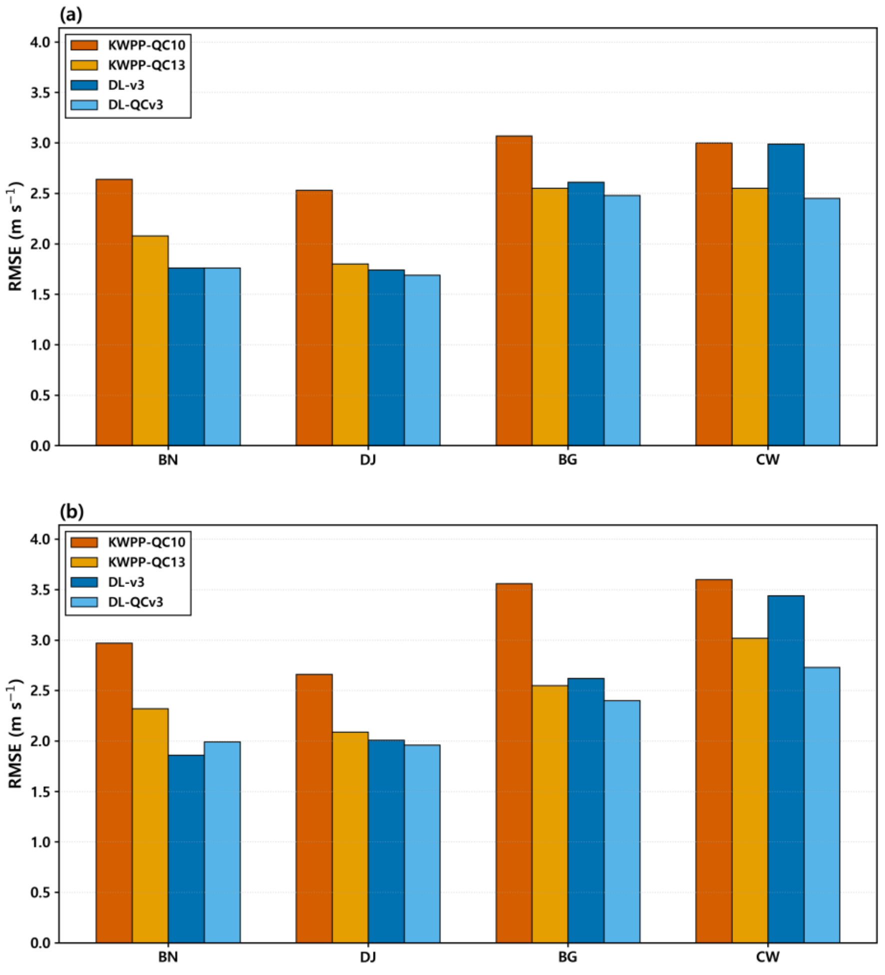

385 **Figure 6. RMSE comparison of KWPP-QC10, KWPP-QC13, DL-v3, and DL-QCv3 for the (a) *u* and (b) *v* wind components across the four observation sites.**

https://doi.org/10.5194/egusphere-2026-3168
Preprint. Discussion started: 25 August 2026

3.3 Restorative Retrieval Characteristics of DL-QCv3

To further investigate the retrieval characteristics associated with the hardware-dependent QC synergy identified in Sect. 3.2, the spatial distribution and quality of wind vectors restored by KWPP-QC13 and DL-QCv3 are examined at BN and DJ, the two 437.5-MHz profiler sites. Although the overall missing data rate at BN and DJ is low (~1 %), these unretrieved points represent complex atmospheric states that serve as critical benchmarks for evaluating the model's capability to reconstruct valid meteorological signals under high ambiguity.

Figure 7 illustrates the distribution of missing wind vectors across the time-altitude domain, where two distinct restorative behaviors emerge based on signal morphology. The first category consists of the DL-recovered regions, which are restored by DL-QCv3, but not by KWPP-QC13. These areas appear as vertically elongated distributions spanning multiple adjacent altitudes at specific timestamps, a pattern that corresponds to the vertically continuous multi-peak phenomenon discussed in Sect. 3.2. While the heuristic logic of KWPP-QC13 fails to isolate the accurate meteorological peak amidst range-smeared interference, DL-QCv3 successfully reconstructs continuous wind structures from these complex spectral environments.

In contrast, the DL-missing regions, where only KWPP-QC13 produced valid retrievals, are horizontally distributed along specific altitudes (approximately 0.7–0.8 km and 1.4–1.5 km) that coincide with typical atmospheric boundary layer heights. These altitudes correspond to atmospheric transition zones near the boundary-layer top, where enhanced vertical wind shear, volume-averaging effects, and range-resolution limitations can increase differences between RWP and RS observations. The concentration of DL-missing regions near these altitudes suggests that DL-QCv3 is more likely to identify retrieval conditions associated with increased spectral ambiguity and designate them as missing, rather than forcing a potentially erroneous retrieval.

https://doi.org/10.5194/egusphere-2026-3168
Preprint. Discussion started: 25 August 2026

Separately, the mutually missing regions labeled "Dupli", where both systems fail to derive wind vectors, are predominantly observed at altitudes above 1.7 km during the winter season. This pattern is fundamentally linked to dry winter atmospheric conditions, where minimal variance in the atmospheric refractive index results in extremely weak SNRs from Bragg scattering, pushing the signals below detectable thresholds. This altitude-dependent data loss reflects the inherent physical limitations of the radar hardware under low-humidity conditions, rather than a deficiency in the retrieval algorithms themselves.

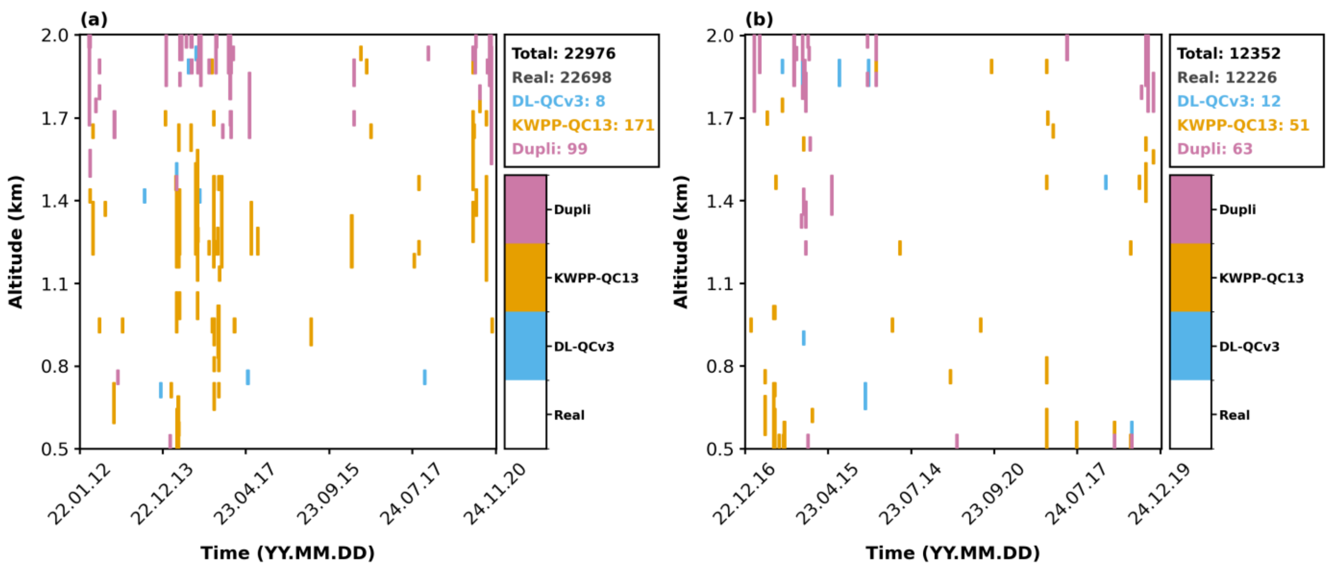

Figure 7. Two-dimensional (time-altitude) missing data regions of wind vectors derived by KWPP-QC13 and DL-QCv3 at the (a) BN and (b) DJ sites.

To quantify the quality of these retrieved wind vectors, error statistics against RS observations are calculated for the respective regions (Figure 8). In the DL-recovered regions (Figure 8a), DL-QCv3 achieves correlation coefficients (R) of 0.84 and 0.92 for the *u* and *v* wind components, respectively. Although the RMSE values (3.07 m s^{-1} for *u* and 4.68 m s^{-1} for *v*) remained relatively large, these elevated errors reflect the inherent complexity of the multi-peak spectral environments targeted in this analysis. Under these highly ambiguous conditions, DL-QCv3 restores over ten times more valid wind vectors than KWPP-QC13 within the affected regions while maintaining relatively strong agreement with the

https://doi.org/10.5194/egusphere-2026-3168
Preprint. Discussion started: 25 August 2026

collocated RS observations. These results suggest that the deep learning framework does not merely perform gap interpolation, but is capable of retrieving wind structures that remain physically consistent with the observed atmospheric flow.

Conversely, the data exclusively retrieved by KWPP-QC13 within the DL-missing regions (Figure 8b) comprises an extremely limited sample size (N = 20). This small number reflects the tendency of DL-QCv3 to conservatively withhold retrievals at physically ambiguous altitudes rather than forcing potentially unreliable derivations. Despite the limited sample size, the KWPP-QC13 retrievals in these regions exhibit weaker agreement with the RS observations than the DL-recovered cases shown in Figure 8a. This behavior suggests that aggressive restoration attempts by conventional heuristic algorithms near atmospheric discontinuities may increase the likelihood of generating physically inconsistent outliers.

Taken together, these findings suggest that DL-QCv3 exhibits environment-dependent retrieval behavior, successfully restoring meteorological wind structures in complex multi-peak spectral environments while conservatively withholding retrievals where physical uncertainty is highest. The following section further examines how these retrieval characteristics vary across seasonal, diurnal, and vertical environments, and discusses the remaining limitations of the proposed framework.

https://doi.org/10.5194/egusphere-2026-3168
Preprint. Discussion started: 25 August 2026

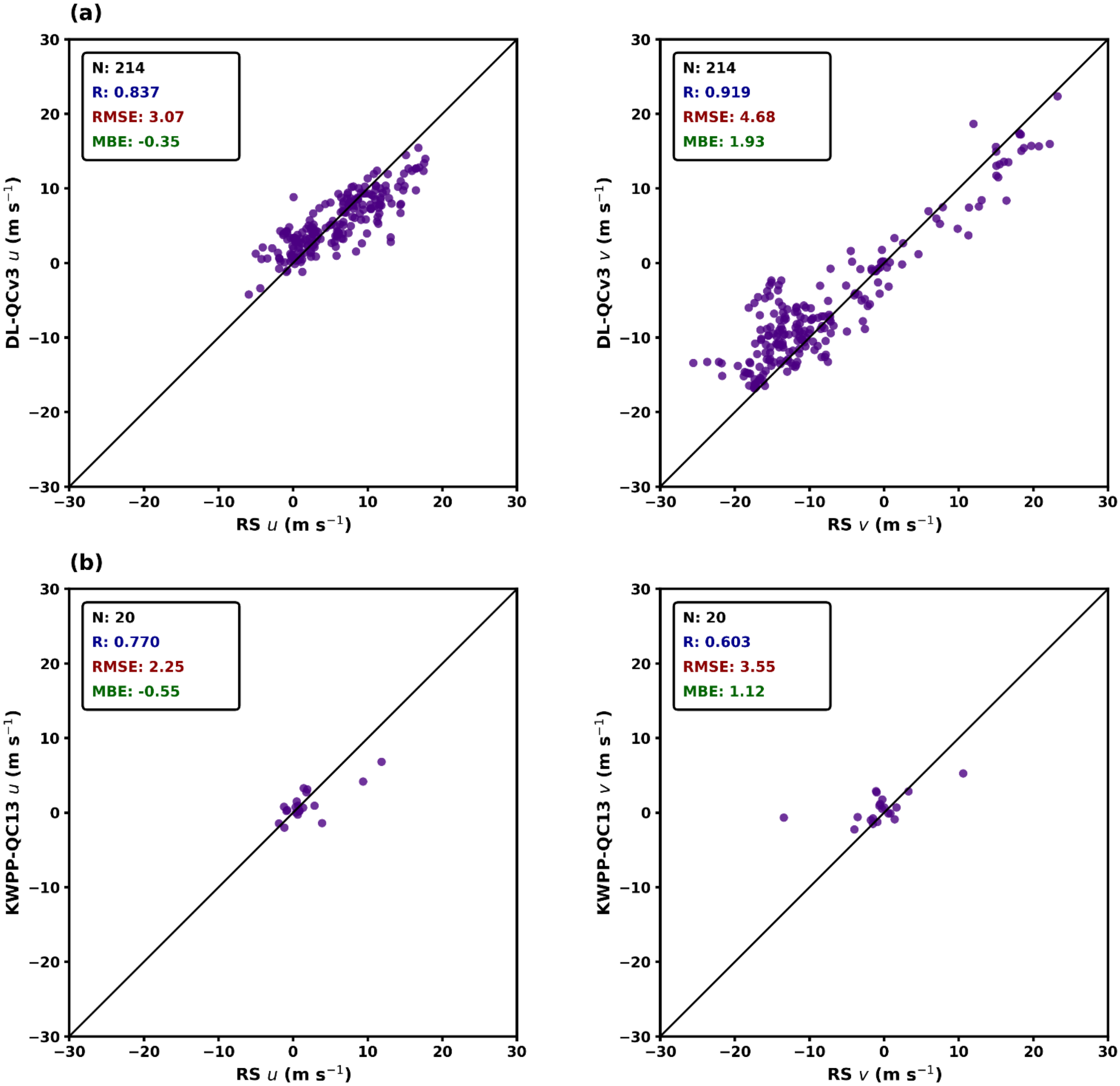

Figure 8. Scatter plots and statistical metrics (R, RMSE, and MBE) of the *u* and *v* wind components compared against RS observations for the regions restored by (a) DL-QCv3 and (b) KWPP-QC13.

https://doi.org/10.5194/egusphere-2026-3168
Preprint. Discussion started: 25 August 2026

3.4 Physical Consistency and Remaining Limitations

3.4.1 Atmospheric Dependence of Retrieval Behavior

To examine whether DL-QCv3 preserves physically meaningful atmospheric and observational characteristics, the monthly, diurnal, and vertical distributions of RMSE and MBE are analyzed at the BN and DJ sites (Figures 9 and 10).

The monthly distributions of RMSE (Figure 9a) reveal a consistent seasonal structure. Retrieval errors are generally larger during winter (December–February) and smaller during summer (June–August). This seasonal dependence is physically expected because warm-season atmospheric conditions enhance Bragg scattering through increased humidity and convective mixing, whereas dry winter conditions reduce refractive-index variability and degrade signal quality. As discussed in Sect. 3.3, the same mechanism contributes to the concentration of mutually missing ("Dupli") regions at higher altitudes during winter. Similar seasonal patterns are also observed in KWPP-QC13, suggesting that the observed seasonality is primarily governed by atmospheric conditions affecting radar signal quality rather than framework-specific behavior. The ability of DL-QCv3 to reproduce this seasonal structure indicates that its retrieval behavior remains physically consistent with the environmental factors controlling retrieval difficulty.

The diurnal distributions (Figure 9b) show that retrieval errors are generally reduced during daytime hours at 06:00 UTC (15:00 KST), when enhanced boundary-layer mixing strengthens Bragg scattering, thereby producing more distinct and spectrally stable meteorological echoes for reliable wind retrieval. In contrast, larger errors are observed during late-night (18:00 UTC; 03:00 KST) and morning-transition periods (00:00 UTC; 09:00 KST), which are characterized by stable stratification and evolving boundary-layer structures. These conditions increase spectral complexity and retrieval difficulty. A notable component-dependent difference emerges at 12:00 UTC (21:00 KST), where the *u* wind component exhibits larger errors than the *v* wind component. This difference may be related to the coastal geometry of the BN and DJ sites. Because the local coastline is oriented primarily in the north–south direction, land–sea-breeze circulations predominantly affect the *u* wind component. At this local time, the transition between sea-breeze and land-breeze regimes can induce rapid directional changes and enhanced vertical shear in the *u*

https://doi.org/10.5194/egusphere-2026-3168
Preprint. Discussion started: 25 August 2026

wind component, thereby increasing representativeness differences between the stationary RWP and drifting RS observations.

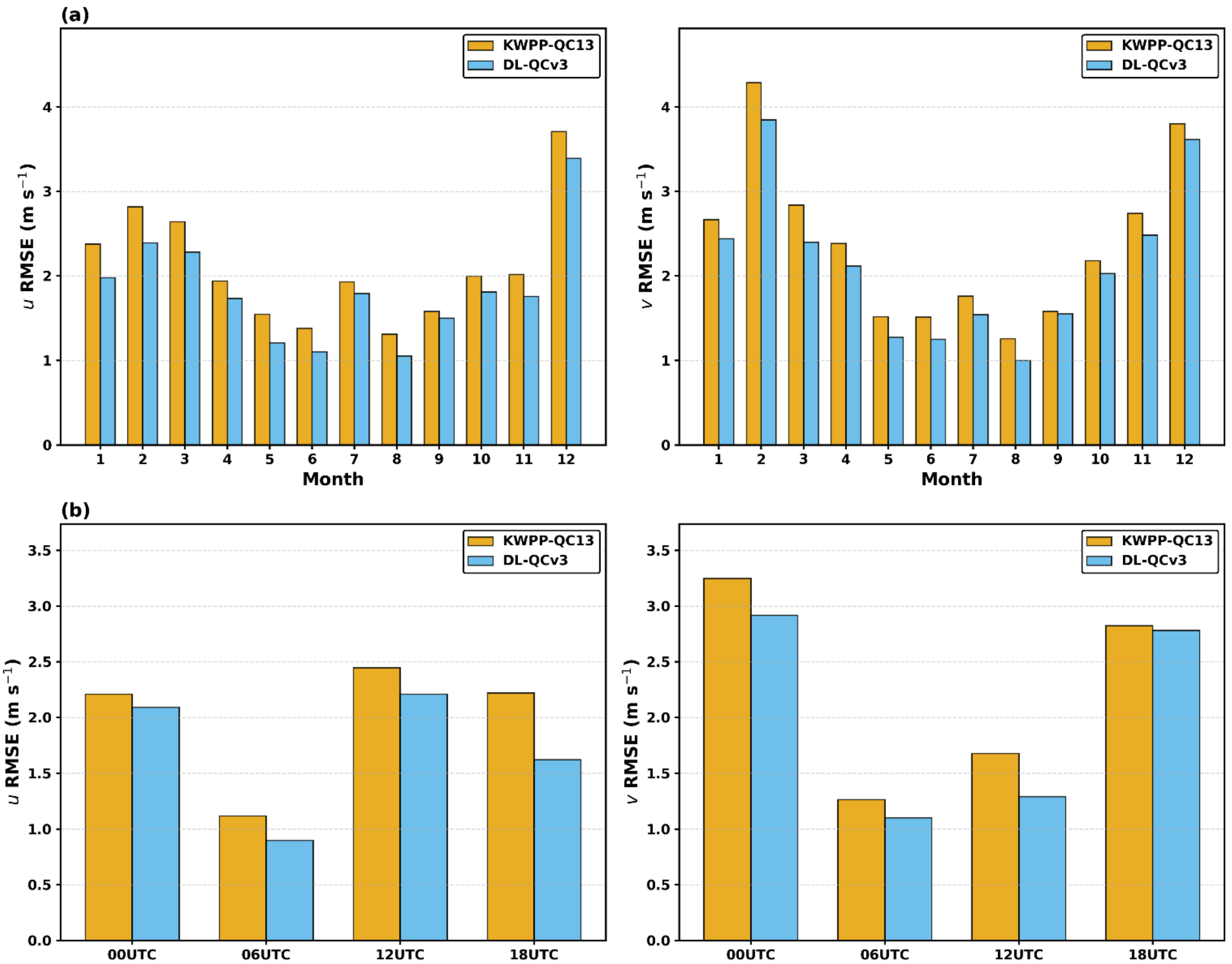

Figure 9. Bar charts of RMSE for the *u* and *v* wind components of KWPP-QC13 and DL-QCv3 over the entire analysis period at the BN and DJ sites, shown by (a) month and (b) observation time (UTC).

The vertical distributions of RMSE and MBE (Figure 10) provide further evidence that the retrieval behavior of DL-QCv3 remains physically consistent across varying atmospheric conditions. Both

https://doi.org/10.5194/egusphere-2026-3168
Preprint. Discussion started: 25 August 2026

frameworks exhibit elevated RMSE and larger MBE magnitudes near altitudes of approximately 0.8 km and 1.4 km, coinciding with the most frequent ABL heights estimated from RS observations (Figure 10, right panels). As discussed in Sect. 3.3, these altitudes correspond to the DL-missing regions where strong vertical gradients amplify representativeness differences between RWP and RS measurements. In addition, MBE of the v wind component exhibits a systematic, altitude-dependent bias shift, transitioning from positive values in the lower layers to negative values aloft. Under the prevailing westerlies of the mid-latitude free atmosphere, variability in the v wind component is relatively limited compared with that of the u wind component. Therefore, the observed altitude-dependent bias likely reflects the increasing spatial separation between the ascending RS and the fixed RWP observation volume with height.

Taken together, the monthly, diurnal, and vertical structures exhibited by DL-QCv3 are consistent with known atmospheric and observational characteristics, supporting the physical consistency of the proposed framework. Nevertheless, several limitations remain under specific observational conditions and are examined in the following section.

https://doi.org/10.5194/egusphere-2026-3168
Preprint. Discussion started: 25 August 2026

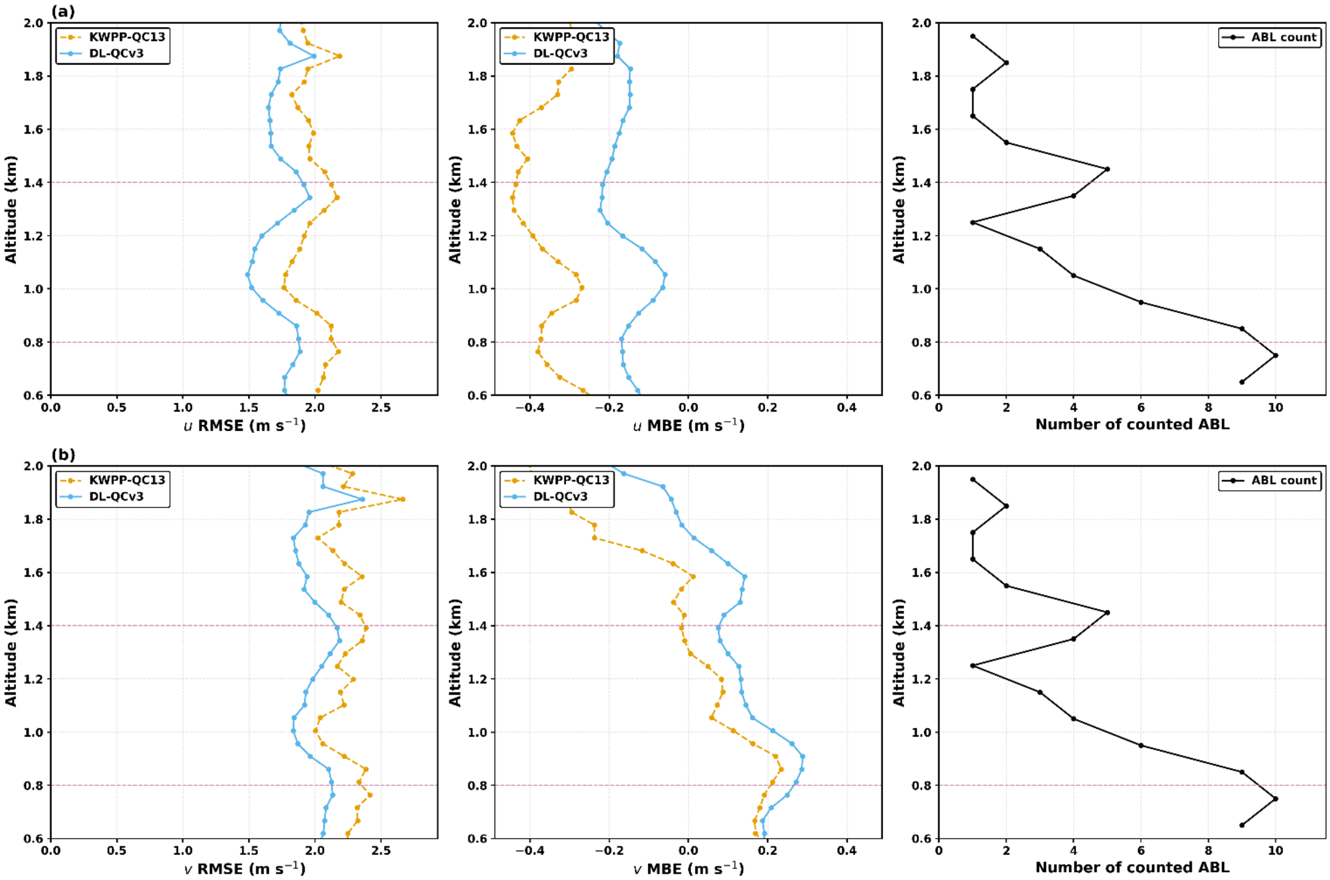

510 **Figure 10. Vertical profiles of RMSE (left column) and MBE (middle column) for the (a) *u* and (b) *v* wind components of KWPP-QC13 and DL-QCv3 at the BN and DJ sites over the entire analysis period. The right column shows the corresponding ABL height frequency distributions derived from RS observations.**

3.4.2 Evaluation of Wind Speed Distribution and Extreme Values

515 To examine whether the physically consistent retrieval behavior identified in Sect. 3.4.1 is maintained across the full wind-speed distribution, including extreme values, quantile–quantile (Q–Q) plots are compared against RS observations (Figure 11).

As shown in Figure 11, DL-QCv3 adheres closely to the 1:1 reference line across the central quantiles of
520 the distribution, indicating reliable agreement with RS observations under typical atmospheric conditions.

https://doi.org/10.5194/egusphere-2026-3168
Preprint. Discussion started: 25 August 2026

However, deviations become increasingly apparent toward the upper and lower tails of the distribution, where DL-QCv3 tends to underestimate the magnitude of extreme wind events.

The tendency to underestimate extreme wind speeds likely reflects the difficulty of representing relatively rare events within a data-driven regression framework. This behavior is consistent with the well-known regression-to-the-mean characteristic of MSE-optimized deep learning models, whereby predictions are drawn toward the center of the training distribution at the expense of rare, high-magnitude events. Consequently, while DL-QCv3 demonstrates reliable performance across the majority of atmospheric conditions, caution may be required when interpreting retrievals associated with rare, high-magnitude wind events.

https://doi.org/10.5194/egusphere-2026-3168
Preprint. Discussion started: 25 August 2026

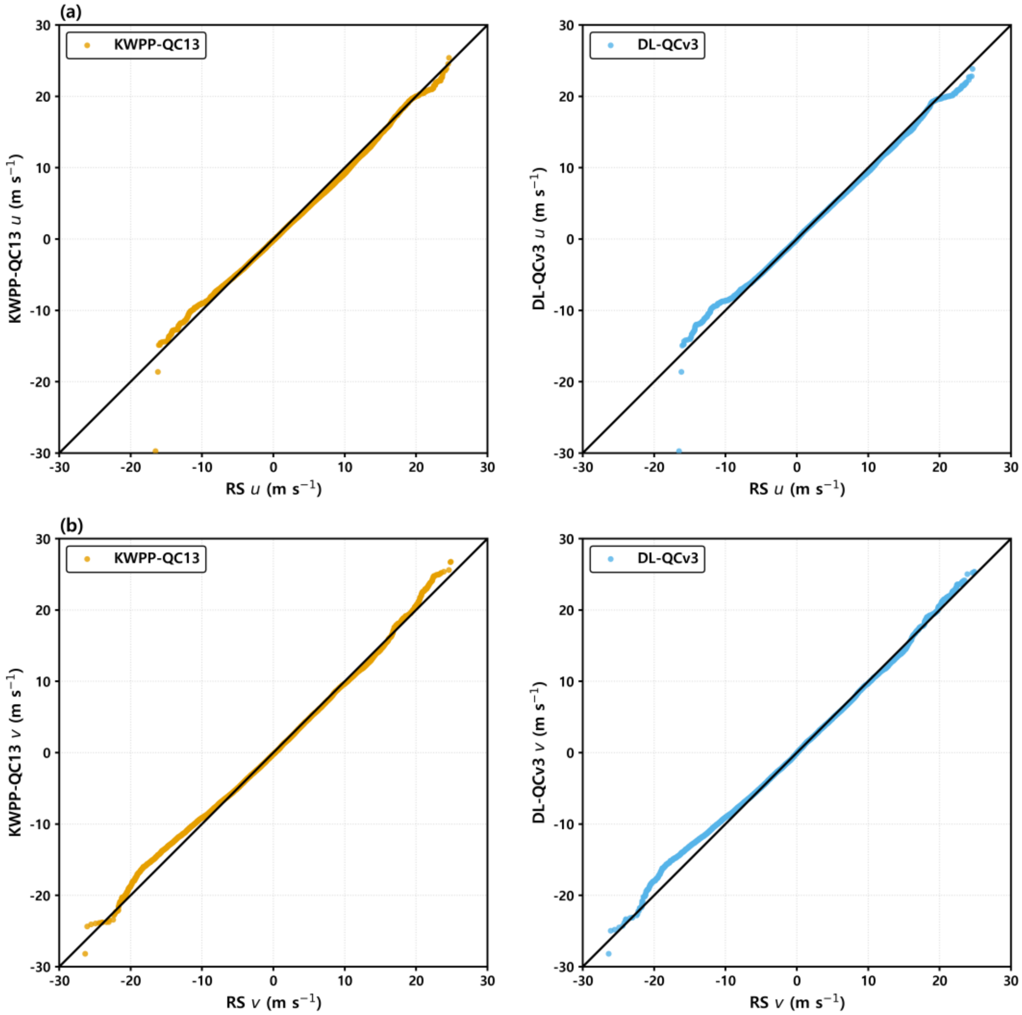

Figure 11. Q-Q plots of the (a) *u* and (b) *v* wind components for KWPP-QC13 and DL-QCv3 against RS observations at the BN and DJ sites.

535

4 Summary and Conclusions

This study develops and validates an end-to-end deep learning framework designed to retrieve wind vectors directly from raw Doppler spectra acquired by RWPs. Using a three-year observational dataset (2022–2024) collected from 437.5-MHz and 1290-MHz profiler systems, the framework is evaluated

https://doi.org/10.5194/egusphere-2026-3168
Preprint. Discussion started: 25 August 2026

under different hardware configurations and signal conditions. The key findings are summarized as follows.

First, the comprehensive model (DL-v3) demonstrates the most robust retrieval performance across all observational sites. By learning from both spectrally reliable and ambiguous samples, DL-v3 maintains strong retrieval performance under favorable signal conditions while substantially reducing systematic bias in complex spectral environments. These results suggest that exploiting the full physical information contained within Doppler spectra is more effective than restricting model training to spectrally pre-filtered subsets, thereby improving retrieval robustness across heterogeneous signal conditions.

Second, the integrated framework (DL-QCv3) demonstrates that the effectiveness of combining deep learning retrieval with conventional post-processing procedures depends strongly on the dominant error characteristics of the radar systems. At the 1290-MHz profiler sites, continuity-based post-processing effectively complements the deep learning retrieval by removing transient outliers associated with non-meteorological echoes. In contrast, at the 437.5-MHz profiler sites, where vertically coherent multi-peak structures induced by range smearing constituted the primary source of uncertainty, additional post-processing provides little benefit beyond the standalone deep learning retrieval. These findings indicate that the effectiveness of combining deep learning with conventional quality-control procedures is not universal, but depends on whether the applied post-processing strategy targets the dominant hardware-induced retrieval errors.

Third, DL-QCv3 demonstrates physically consistent retrieval behavior beyond simple improvements in statistical performance. In complex multi-peak environments, the framework restores more than ten times the number of valid wind vectors compared with KWPP-QC13 while maintaining strong agreement with RS observations. Furthermore, DL-QCv3 reproduced physically meaningful seasonal, diurnal, and vertical retrieval characteristics associated with variations in signal quality, boundary-layer-related retrieval difficulty, and observational representativeness effects. These results suggest that the proposed framework preserves key atmospheric and observational dependencies governing wind retrieval behavior.

https://doi.org/10.5194/egusphere-2026-3168
Preprint. Discussion started: 25 August 2026

Despite these advantages, the analysis of wind-speed distributions revealed a tendency to underestimate extreme wind events. This behavior reflects the well-known regression-to-the-mean characteristic of deep learning models trained using mean-squared-error-based optimization and remains a limitation when retrieving rare high-magnitude winds.

In conclusion, this study demonstrates that deep learning provides a robust and operationally viable framework that can function either as a standalone alternative to conventional spectral quality-control pipelines or be selectively integrated with conventional post-processing procedures for complementary benefits. Beyond improving retrieval accuracy and data availability, the proposed framework provides new insight into how radar hardware characteristics, spectral ambiguities, and atmospheric variability interact within a deep learning-based retrieval system. The results offer practical guidance for the hardware-aware application of deep learning in future operational RWP processing frameworks.

https://doi.org/10.5194/egusphere-2026-3168
Preprint. Discussion started: 25 August 2026

Code availability

The codes developed for this study are not publicly available but can be provided by the corresponding authors upon reasonable request.

Data availability

The radar wind profiler and radiosonde observations used in this study were provided by the Korea Meteorological Administration (KMA). The data are subject to KMA data access policies and cannot be redistributed by the authors.

Author contributions

K.H.L. designed the research, performed the data analysis, and prepared the manuscript. R.H.S. designed the deep learning model, acquired the funding, and critically reviewed the manuscript. B.H.K. supervised the research and critically reviewed the manuscript. All authors read and approved the final manuscript.

Competing interests

The authors declare that they have no conflict of interest.

Acknowledgements

The authors thank the Weather Radar Center of the Korea Meteorological Administration (KMA) for providing the radar wind profiler and radiosonde observations used in this study. Artificial intelligence tools (ChatGPT, Claude, and Gemini) were used solely for English language editing and proofreading.

Financial support

This work was funded by the Korea Meteorological Administration Research and Development Program under Grant RS-2024-00404042 and the National Research Foundation of Korea (NRF) grant funded by the Korea government (MSIT) (RS-2024-00343921).

https://doi.org/10.5194/egusphere-2026-3168
Preprint. Discussion started: 25 August 2026

References

Boisse, J., Klaus, V., and Aubagnac, J.: A wavelet transform technique for removing airplane echoes from ST radar signals, J. Atmos. Ocean. Technol., 16, 334–346, doi: https://doi.org/10.1175/1520-0426(1999)016<0334:AWTTFR>2.0.CO;2, 1999.

Brett, A. C. and Tuller, S. E.: The autocorrelation of hourly wind speed observations, Journal of Applied Meteorology (1988-2005), 823–833, doi: https://doi.org/10.1175/1520-0450(1991)030<0823:TAOHWS>2.0.CO;2, 1991.

Carter, D. A., Gage, K. S., Ecklund, W. L., Angevine, W. M., Johnston, P. E., Riddle, A. C., Wilson, J., and Williams, C. R.: Developments in UHF lower tropospheric wind profiling at NOAA's Aeronomy Laboratory, Radio Sci., 30, 977–1001, doi: https://doi.org/10.1029/95RS00649, 1995.

Chen, Z., Chu, Y., and Su, C.: Intercomparisons of tropospheric wind velocities measured by multi-frequency wind profilers and rawinsonde, Atmosphere, 12, 1284, https://doi.org/10.3390/atmos12101284, 2021.

Clevert, D., Unterthiner, T., and Hochreiter, S.: Fast and accurate deep network learning by exponential linear units (elus), arXiv preprint arXiv:1511.07289, 4, 11, 2015.

Clothiaux, E. E., Penc, R. S., Thomson, D. W., Ackerman, T. P., and Williams, S. R.: A first-guess feature-based algorithm for estimating wind speed in clear-air Doppler radar spectra, J. Atmos. Ocean. Technol., 11, 888–908, doi: https://doi.org/10.1175/1520-0426(1994)011<0888:AFGFBA>2.0.CO;2, 1994.

Cohn, S. A., Brown, W., Martin, C. L., Susedik, M. E., Maclean, G. D., and Parsons, D. B.: Clear air boundary layer spaced antenna wind measurement with the Multiple Antenna Profiler (MAPR), in: Annales Geophysicae, 845–854, 2001.

Cornman, L. B., Goodrich, R. K., Morse, C. S., and Ecklund, W. L.: A fuzzy logic method for improved moment estimation from Doppler spectra, J. Atmos. Ocean. Technol., 15, 1287–1305, doi: https://doi.org/10.1175/1520-0426(1998)015<1287:AFLMFI>2.0.CO;2, 1998.

DesRosiers, A. J. and Bell, M. M.: Airborne radar quality control with machine learning, Artificial Intelligence for the Earth Systems, 3, e230064, doi: https://doi.org/10.1175/AIES-D-23-0064.1, 2024.

https://doi.org/10.5194/egusphere-2026-3168
Preprint. Discussion started: 25 August 2026

Fischler, M. A. and Bolles, R. C.: Random sample consensus: a paradigm for model fitting with applications to image analysis and automated cartography, Commun ACM, 24, 381–395, doi: https://doi.org/10.1145/358669.358692, 1981.

Gage, K. S. and Balsley, B. B.: Doppler radar probing of the clear atmosphere, Bull. Am. Meteorol. Soc., 59, 1074–1094, doi: https://doi.org/10.1175/1520-0477(1978)059<1074:DRPOTC>2.0.CO;2, 1978.

Goodrich, R. K., Morse, C. S., Cornman, L. B., and Cohn, S. A.: A horizontal wind and wind confidence algorithm for Doppler wind profilers, J. Atmos. Ocean. Technol., 19, 257–273, doi: https://doi.org/10.1175/1520-0426-19.3.257, 2002.

Griesser, T. and Richner, H.: Multiple peak processing algorithm for identification of atmospheric signals in Doppler radar wind profiler spectra, Meteorologische Zeitschrift, 7, doi: https://doi.org/10.1127/metz/7/1998/292, 1998.

Haefele, A. and Ruffieux, D.: Validation of the 1290 MHz wind profiler at Payerne, Switzerland, using radiosonde GPS wind measurements, Meteorol. Appl., 22, 873–878, doi: https://doi.org/10.1002/met.1507, 2015.

Hildebrand, P. H. and Sekhon, R. S.: Objective determination of the noise level in Doppler spectra, Journal of Applied Meteorology and Climatology, 13, 808–811, doi: https://doi.org/10.1175/1520-0450(1974)013<0808:ODOTNL>2.0.CO;2, 1974.

Holleman, I.: Quality control and verification of weather radar wind profiles, J. Atmos. Ocean. Technol., 22, 1541–1550, doi: https://doi.org/10.1175/JTECH1781.1, 2005.

Ingleby, B., Pauley, P., Kats, A., Ator, J., Keyser, D., Doerenbecher, A., Fucile, E., Hasegawa, J., Toyoda, E., and Kleinert, T.: Progress toward high-resolution, real-time radiosonde reports, Bull. Am. Meteorol. Soc., 97, 2149–2161, doi: https://doi.org/10.1175/BAMS-D-15-00169.1, 2016.

Ioffe, S. and Szegedy, C.: Batch normalization: Accelerating deep network training by reducing internal covariate shift, in: International conference on machine learning, 448–456, 2015.

Jordan, J. R., Lataitis, R. J., and Carter, D. A.: Removing ground and intermittent clutter contamination from wind profiler signals using wavelet transforms, J. Atmos. Ocean. Technol., 14, 1280–1297, doi: https://doi.org/10.1175/1520-0426(1997)014<1280:RGAICC>2.0.CO;2, 1997.

https://doi.org/10.5194/egusphere-2026-3168
Preprint. Discussion started: 25 August 2026

Kottayil, A., Mohanakumar, K., Samson, T., Rebello, R., Manoj, M. G., Varadarajan, R., Santosh, K. R., Mohanan, P., and Vasudevan, K.: Validation of 205 MHz wind profiler radar located at Cochin, India, using radiosonde wind measurements, Radio Sci., 51, 106–117, https://doi.org/10.1002/2015RS005836, 2016.

Kretzschmar, R., Karayiannis, N. B., and Richner, H.: Removal of bird-contaminated wind profiler data based on neural networks, Pattern Recognit, 36, 2699–2712, doi: https://doi.org/10.1016/S0031-3203(03)00165-1, 2003.

Lambert, W. C., Merceret, F. J., Taylor, G. E., and Ward, J. G.: Performance of five 915-MHz wind profilers and an associated automated quality control algorithm in an operational environment, J. Atmos. Ocean. Technol., 20, 1488–1495, doi: https://doi.org/10.1175/1520-0426(2003)020<1488:POFMWP>2.0.CO;2, 2003.

Lee, K. H., Kwon, B. H., Lee, J. H., Yoon, S. J., Kwon, S. H., and Jung, S. H.: Standardized radar wind profiler dataset via integrated raw data processing in Korea, Sci. Data, https://doi.org/10.1038/s41597-026-07277-1, 2026.

Lehmann, V. and Teschke, G.: Advanced intermittent clutter filtering for radar wind profiler: Signal separation through a Gabor frame expansion and its statistics, in: Annales Geophysicae, 759–783, 2008.

Liu, B., Ma, X., Guo, J., Wen, R., Li, H., Jin, S., Ma, Y., Guo, X., and Gong, W.: Extending the wind profile beyond the surface layer by combining physical and machine learning approaches, Atmospheric Chemistry and Physics, 24, 4047–4063, doi: https://doi.org/10.5194/acp-24-4047-2024, 2024.

Lolli, S.: Machine learning techniques for vertical lidar-based detection, characterization, and classification of aerosols and clouds: A comprehensive survey, Remote Sensing, 15, 4318, doi: https://doi.org/10.3390/rs15174318, 2023.

Meng, D., Guo, J., Chen, J., Guo, X., Li, N., Sun, Y., Zhang, Z., Tang, N., Xu, H., and Chen, T.: Low-level atmospheric turbulence dataset in China generated by combining radar wind profiler and radiosonde observations, Earth System Science Data, 17, 4023–4037, doi: https://doi.org/10.5194/essd-17-4023-2025, 2025.

https://doi.org/10.5194/egusphere-2026-3168
Preprint. Discussion started: 25 August 2026

Merritt, D. A.: A statistical averaging method for wind profiler Doppler spectra, J. Atmos. Ocean. Technol., 12, 985–995, doi: https://doi.org/10.1175/1520-0426(1995)012<0985:ASAMFW>2.0.CO;2, 1995.

Petersen, R. A. and Bedka, K. M.: Determining the accuracy and representativeness of wind profiler data, in: Preprints, 11th Symp. on Integrated Observing and Assimilation Systems for the Atmosphere, Oceans, and Land Surface, San Antonio, TX, Amer. Meteor. Soc, 2007.

Petitdidier, M., Sy, A., Garrouste, A., and Delcourt, J.: Statistical characteristics of the noise power spectral density in UHF and VHF wind profilers, Radio Sci., 32, 1229–1247, doi: https://doi.org/10.1029/97RS00250, 1997.

St-James, J. S. and Laroche, S.: Assimilation of wind profiler data in the Canadian Meteorological Centre’s analysis systems, J. Atmos. Ocean. Technol., 22, 1181–1194, doi: https://doi.org/10.1175/JTECH1765.1, 2005.

Strauch, R. G., Merritt, D. A., Moran, K. P., Earnshaw, K. B., and De Kamp, D. V.: The Colorado wind-profiling network, J. Atmos. Ocean. Technol., 1, 37–49, doi: https://doi.org/10.1175/1520-0426(1984)001<0037:TCWPN>2.0.CO;2, 1984.

Thomann, G. C. and Barfield, M. J.: The time variation of wind speeds and windfarm power output in Kansas, IEEE Trans. Energy Convers., 3, 44–49, doi: https://doi.org/10.1109/60.4198, 1988.

Tong, Z., Liu, B., Ma, X., Li, H., Wei, R., and Gong, W.: Estimation of boundary layer height from radar wind profiler by deep learning algorithms, IEEE Trans. Geosci. Remote Sens., 62, 1–11, doi: https://doi.org/10.1109/TGRS.2024.3434403, 2024.

Weber, B. L., Wuertz, D. B., Welsh, D. C., and McPeek, R.: Quality controls for profiler measurements of winds and RASS temperatures, J. Atmos. Ocean. Technol., 10, 452–464, doi: https://doi.org/10.1175/1520-0426(1993)010<0452:QCFPMO>2.0.CO;2, 1993.

Weisshaupt, N., Lehmann, V., Arizaga, J., and Maruri, M.: Radar wind profilers and avian migration: a qualitative and quantitative assessment verified by thermal imaging and moon watching, Methods in Ecology and Evolution, 8, 1133–1145, doi: https://doi.org/10.1111/2041-210X.12763, 2017.

Wilczak, J. M., Strauch, R. G., Ralph, F. M., Weber, B. L., Merritt, D. A., Jordan, J. R., Wolfe, D. E., Lewis, L. K., Wuertz, D. B., and Gaynor, J. E.: Contamination of wind profiler data by migrating birds:

https://doi.org/10.5194/egusphere-2026-3168
Preprint. Discussion started: 25 August 2026

Characteristics of corrupted data and potential solutions, J. Atmos. Ocean. Technol., 12, 449–467, doi: https://doi.org/10.1175/1520-0426(1995)012<0449:COWPDB>2.0.CO;2, 1995.

Woodman, R. F.: Spectral moment estimation in MST radars, Radio Sci., 20, 1185–1195, doi: https://doi.org/10.1029/RS020i006p01185, 1985.